ACS APPLIED MATERIALS & INTERFACES

Research Article

www.acsami.org

Synthesis and Photovoltaic Properties of Novel Monoadducts and Bisadducts Based on Amide Methanofullerene

Chao Liu,[†,‡] Shengqiang Xiao,*[,§] Xiangping Shu,[§] Yongjun Li,[†] Liang Xu,[†,‡] Taifeng Liu,[†,‡] Yanwen Yu,[†,‡] Liang Zhang,[⊥] Huibiao Liu,[†] and Yuliang Li*[,†]

[†]Beijing National Laboratory for Molecular Sciences (BNLMS), CAS Key Laboratory of Organic Solids, Institute of Chemistry, Chinese Academy of Sciences, Beijing 100190, P. R. China

[‡]Graduate University of Chinese Academy of Sciences, Beijing 100190, P. R. China

[§]State Key Laboratory of Advanced Technology for Materials Synthesis and Processing, WUT-USG Joint Laboratory of Advanced Optoelectronic Materials and Devices, Wuhan University of Technology, Luoshi Road 122, Wuhan 430070, China

[⊥]Shandong Normal University, Jinan, 250014, P. R. China

Supporting Information

ABSTRACT: Four new [6,6]-phenyl-C_{61} and C_{71} butylsaure *n*-dibutyl amides (PCBDBA) with mono- and bis-adduction on C_{60} and C_{70} cages, respectively, have been synthesized as models to study the effect of the mono- and bis-adduction on fullerene cages on device performance when used as electron acceptors with the donor of regioregular P3HT in bulkheterojunction organic photovoltaics (BHJ-OPV). The optoelectronic, electrochemistry, and photovoltaic properties of these mono- and bis-products were fully investigated. The best device performance of these fullerene derivatives were obtained from the two monoadducts with power conversion efficiency (PCE) of 1.77% for C_{60} derivative and 1.90% for C_{70} derivative, respectively, which are close to PCBM's 2.43%. The results revealed the structure−function relationship among the monoadduct and bisadduct derivatives of C_{60} and C_{70} with the BHJ-OPV performance.

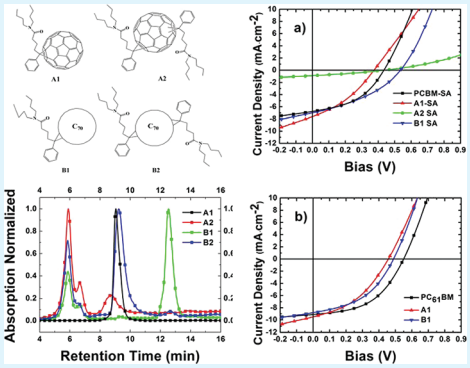

KEYWORDS: *fullerene, photovoltaic, solar cell, C_{60}, C_{70}*

INTRODUCTION

To achieve high power conversion efficiency (PCE), great research efforts have been focused on designing and synthesizing new polymers for fullerene-polymer blended bulk heterojunction organic photovoltaics (BHJ-OPVs),[1−7] and new materials with PCE of 9.2% were generated.[8] Among the acceptor materials used in OPVs, [6,6]-phenyl C_{61}-butyric acid methyl ester ($PC_{61}BM$) plays a dominant role due to its advantages of good solubility in organic solvents, high electron mobility, high electron affinity, and ease of preparation at low cost. However, the weak absorption in the visible region and lower-lying LUMO level are shortcomings. Weak absorption in the visible region limits its contribution to the light harvest in the photovoltaic conversion.[9] Lower-lying LUMO level of an acceptor material results in lower open circuit voltage (V_{oc}) of OPVs because V_{oc} is related to the gap between the LUMO of the acceptor and the HOMO of the donor in a BHJ-OPV device.[10] Although many alternative structures to PCBM have been synthesized and used as acceptors in OPVs, most of their performances could not outperform PCBM.[11−17] A few showed better performance but with limited successful applications with donor polymers or need additional device fabrication techniques.[9,18−20]

$PC_{71}BM$ was an electron acceptor with higher photovoltaic performance in BHJ-OPVs, attributed to higher molar extinction coefficient in the visible region due to asymmetric C_{70} core.[4,9,21] Aromatic groups attached to fullerenes by covalent or conjugated linkage can increase the molar absorption of fullerene derivatives and decrease the number of π electrons of the fullerene core which weakens the ability of accepting electrons and then increases LUMO level.[22] Therefore, the LUMO level of [6,6] isomers (methanofullerenes) with 58 π electrons was higher than that of [5,6] isomers (fulleroids) with 60 π electrons. Moreover, with fewer π electrons on fullerene core, the higher LUMO level can be obtained with more adducts.[23,24] Multiadducted PCBM mixtures used as acceptors in BHJ-OPV were first reported by Padinger et al.;[25] low performance and J_{sc} were obtained using doctor blade technology for device fabrication. Afterward, Lenes et al.[26] studied the physical and photovoltaic properties of several bisadducts of $PC_{61}BM$-like derivatives and the triadduct of $PC_{61}BM$. They found that the higher LUMO level and V_{oc} of the derivatives can be obtained with more

Received: December 1, 2011
Accepted: January 2, 2012
Published: January 2, 2012

ACS Publications © 2012 American Chemical Society

dx.doi.org/10.1021/am2016975 | *ACS Appl. Mater. Interfaces* 2012, 4, 1065−1071

adductions, but the J_{sc} decreased, especially for the triadduct of $PC_{61}BM$. They attributed the low J_{sc} to the decreased electron mobility of derivatives with higher adductions.[26,27]

Understanding the structure−function relationships that relate specifically to fullerene derivatives could lead to new "design rules" for producing benign, high-performance photovoltaic devices. Our studies focused on fullerene physics and chemistry and were dedicated to develop low cost, ease of preparation, and high performance fullerene materials for photovoltaic application in recent years.[15,28−30] In the present work, we reported our detailed optoelectronic, electrochemistry, photovoltaic, and morphology study on a series of fullerene materials, [6,6]-phenyl-C_{61} or C_{71} butylsaure *n*-dibutyl amides (PCBDBA), which were N,N-disubstituted amide analog of PCBM with higher solubility than PCBM. As a continuation to our previous work,[15] C_{60}, C_{70}, and their bisadducted derivatives, i.e., fullerenes **A1**, **A2**, **B1**, and **B2** as shown in Figure 1, were designed and synthesized . They were

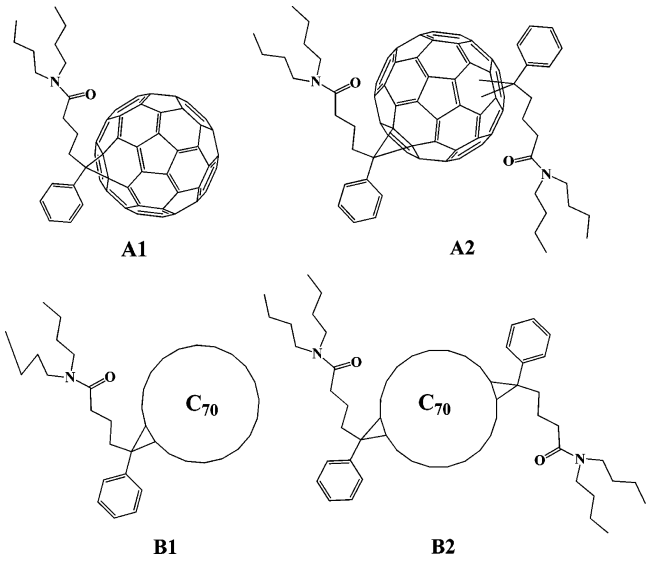

Figure 1. Structures of 4 fullerene derivatives.

good models to study the influence of the bisadducted fullerene materials on the performance of bulk heterojunction organic photovoltaics, to reveal the structure−function relationship of C_{60} and C_{70} monoadducts and bisadducts on the photovoltaics performance and provide the logos on how to design fullerene materials for this purpose.

EXPERIMENTAL SECTION

General. All solvents were purified and freshly distilled prior to use according to literature procedures and purification handbook. Commercially available materials were used as received. Styles of equipment and reagents were shown in Table S7s and S8 in the Supporting Information.

Synthesis and Characterization. The PCBDBA series were synthesized according to the method developed by Hummelen et al.[31] (Scheme S1, Supporting Information). General method for a diazomethane addition to fullerene: A mixture of hydrazone (1 mmol), freshly prepared sodium methoxide (1.2 mmol), and dry pyridine (15 mL) was placed under nitrogen and stirred at room temperature for 15−30 min. Then, a solution of fullerene (1 mmol) in dry 1,2-dichlorobenzene (*o*-DCB, 50 mL) was added. The mixture was stirred at 80−120 °C for 12−24 h, and then, the solvent was removed in vacuo. The crude product was purified by chromatography on silica gel (200−300 mesh) with 0−50% ethyl acetate in toluene as the eluent. Every portion of different adducts were collected and then redissolved in *o*-DCB and refluxed for 24 h to ensure most of [5,6] open shell isomers converted to [6,6] close shell methanofullerenes. After removing *o*-DCB in vacuo, the product was purified by chromatograph on silica gel (300−400 mesh) two times to remove some decomposed compounds and other fullerene impurities. Then, the product was dissolved in a little dichloromethane and precipitated with MeOH, centrifuged, and decanted. The remaining pellet was washed three times with methanol, hexane, or Et_2O, respectively, in a supersonic bath to remove small molecule impurities and silicon gel. Finally, all materials were dried in vacuo at 100 °C for 24 h, resulting in as pure [6,6]methanofullerene derivatives as possible.

^1H NMR and ^{13}C NMR spectra were calibrated using signals from trimethylsilane (TMS) and reported downfield from TMS. Matrix-assisted laser desorption ionization time-of-flight mass spectrometry (MALDI-TOF-MS) gave the M^-, according to the calculated value of m/z of all the C_{60} and C_{70} derivatives. The FT-IR spectra showed absorption features at 526 cm^{-1} c.a. indicative of the C_{60} core, while 578 cm^{-1} and 534 cm^{-1} for the C_{70} core.

A1. Monoadduct: Yield, 30%; ^1H NMR ($CDCl_3$, 400 MHz): δ (ppm): 7.94 (2 H, d, J = 7.4 Hz), 7.53 (2 H, t, J = 7.4 Hz), 7.43 (1 H, t, J = 7.16 Hz), 3.30 (2 H, t, 7.6 Hz), 3.20 (2 H, t, J = 8.0 Hz), 2.93 (2 H, t, J = 8.0 Hz), 2.50 (2 H, t, J = 7.7 Hz), 2.22 (2 H, m), 1.51 (4 H, m), 1.29 (4 H, m), 0.92 (6 H, m). ^{13}C NMR (100 MHz, $CDCl_3$): δ (ppm): 171.38, 149.02, 148.14, 146.06, 145.36, 145.30, 145.25, 145.21, 144.96, 144.94, 144.82, 144.65, 144.60, 144.21, 143.94, 143.22, 143.17, 143.15, 143.10, 142.40, 142.33, 142.32, 142.29, 141.16, 140.95, 138.21, 137.79, 136.99, 132.32, 128.62, 128.36, 80.18, 52.44, 48.01, 46.00, 34.23, 33.29, 31.54, 30.26, 23.05, 20.72, 20.63, 14.29, 14.28. IR (KBr) = ν (cm^{-1}): 3297 (w), 2954 (s), 2953 (s), 2864 (m), 1644 (s), 1450 (m), 1426 (m), 1375 (w), 1210 (w), 1184 (w), 1136(w), 752 (m), 710 (m), 577 (w), 551 (w), 527 (m, C_{60} feature). MALDI-TOF CCA m/z: 1007.3 (M^-); calcd. ($C_{79}H_{29}NO$), 1007.22.

A2. Bisadduct: Yield, 30%; ^1H NMR ($CDCl_3$, 400 MHz): δ (ppm): 8.26−7.70 (2 H, m), 7.68−7.34 (3 H, m), 3.42−2.86 (4 H, m), 2.65−1.87 (4 H, m), 1.82−1.03 (10 H, m), 1.03−0.58 (6 H, m). IR (KBr) = ν (cm^{-1}): 3368 (w), 2956 (s), 2900 (s), 2856 (s), 1739 (m), 1645 (s), 1460 (s), 1377 (m), 1289 (w), 1258 (w), 1214 (w), 1142 (w), 1085 (w), 1020 (w), 850 (w), 760 (w), 735 (w), 702 (w), 525 (m), 463 (w, C_{60} feature). MALDI-TOF CCA m/z: 1007.3 (M^-); MALDI-TOF CCA m/z: 1295.1 (M^-); calcd. ($C_{98}H_{58}N_2O_2$), 1295.45.

B1. Monoadduct: Yield 20%; ^1H NMR (400 MHz, $CDCl_3$): δ (ppm): ^1H NMR (400 MHz, $CDCl_3$): δ (ppm): 8.08−7.75 (2 H, m), 7.58−7.46 (2 H, m), 7.45−7.37 (1 H, m) 3.56−2.93 (4 H, m), 2.54−2.36 (4 H, m), 2.31−1.75 (2 H, m), 1.51 (4 H, s), 1.42−1.11 (4 H, m), 1.03−0.80 (6 H, m). IR (KBr) = ν (cm^{-1}): 3445 (w), 2952 (m), 2923 (m), 2855 (m), 1644 (s), 1557 (w), 1539 (w), 1454 (m), 1428 (s, C_{70} feature), 1374 (w), 1289(w), 1213 (w), 1135 (w), 1073 (w), 841 (w), 795 (w), 727 (w), 674 (w), 643 (w), 578 (m, C_{70} feature), 534 (m, C_{70} feature), 458 (w). MALDI-TOF CCA m/z: 1007.3 (M^-); MALDI-TOF CCA m/z: Monoadduct, 1127.5 (M^-); calcd. ($C_{79}H_{29}NO$), 1127.22.

B2. Bisadduct: Yield, 15%; ^1H NMR (600 MHz, $CDCl_3$): δ(ppm): 8.04−7.90 (2 H, m), 7.61−7.32 (3 H, m), 3.39−3.11 (4 H, m), 2.61−2.29 (4 H, m), 2.27−1.98 (2 H, m), 1.66−1.45 (4 H, m), 1.39−1.16 (m, 4 H), 1.02−0.76 (6 H, m). IR (KBr) = ν (cm^{-1}): 3421 (mb), 2958 (s), 2926 (s), 2856 (m), 1647 (s), 1456 (m), 1440 (m), 1425 (m, C_{70} feature), 1383 (m), 1261 (m), 1095 (m), 1028 (m), 862 (w), 804 (m), 801 (w), 646 (w), 578 (w, C_{70} feature), 535 (w, C_{70} feature), 458 (w), 419 (w). MALDI-TOF CCA m/z: 1007.3 (M^-); MALDI-TOF CCA m/z: 1416.1(M^-); calcd. ($C_{98}H_{58}N_2O_2$), 1415.45.

All fullerene multiadducts are complicated mixtures of isomers, while for C_{70}, with a lower symmetry than C_{60}, a mixture of isomers of monoadduct also formed.[26] Herein, ^{13}C NMR are unable to give exact information, because there are hundreds of signals from the fullerene and aromatic moiety to be assigned; the multiadduct can be analyzed by HPLC on analytical Cosmosil Buckyprep Waters column, i.e., 4.6 mm (ID) × 250 mm column, using toluene as eluent at a flow rate of 0.6 mL/min, to give some information about the minimum number of isomers; however, it seemed difficult to indicate how many isomers

there were even though 5PYE or 5PBB analytical column was used. The resulting chromatograms (320 nm detection) of the four were showed in Figure 2, and isomer integration was listed in Table S2, Supporting Information, which suggested that there were at least 3 isomers of **A2**, 5 isomers of **B1**, and 5 isomers of **B2**.

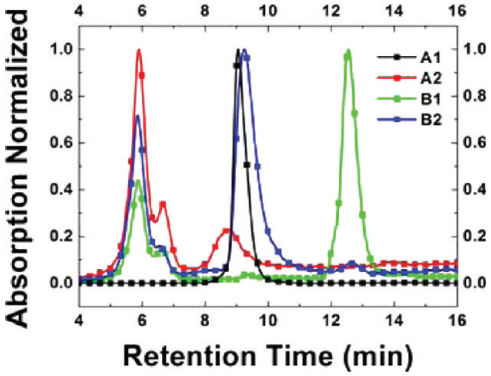

Figure 2. HPLC analysis figures of four fullerene derivatives. LC: Waters 699; column: Cosmosil Buckyprep Waters 4.6 mm(ID) × 250 mm; eluent: HPLC grade toluene; flow rate: 0.6 mL/min; detection wavelength: 320 nm; neither recycle nor another special technique was used; and the retention time of C_{60} in this condition was 13.3 min and 21.7 min for C_{70}.

Thermal Analysis. Samples were kept at 100 °C in vacuo for 24 h before thermal analysis. Thermogravimetric/differential thermal analysis (TG/DTA) was measured to understand the thermal stability of the fullerene derivatives as shown in Table S1, Supporting Information, which indicates that all fullerene derivatives have a thermal decomposition temperature higher than 200 °C. Differential scanning calorimetry (DSC) measurement of them showed that there were no crystallization temperatures (T_c) under 200 °C, but **A1** has a melting temperature (T_m) at 239 °C (peak); **B1** has T_g at 128 °C and T_m at 219 °C (Figure S4, Supporting Information, the peak at 196 °C was transition phase between the melting phase and glass phase), which suggested that all four fullerene derivatives are amphorous materials.[32]

Photovoltaic Fabrication. The device structure used in this study was a classic sandwich structure with ITO/PEDOT:PSS as a hole-collecting electrode and Al as an electron-collecting electrode (Figure S5, Supporting Information). Indium/tin oxide (ITO, 150 nm thick) glasses were cleaned by supersonic treatment in acetone, water, acetone, and *i*-propanol for at least 10 min, respectively and then by UV/ozone treatment for 20 min and used as the anode. A thin layer of poly (ethylene dioxythiophene):polystyrenesulfonic acid (PEDOT:PSS, CLEVIOS PH750) was incorporated between the ITO and the active layer to reduce device leakage, which was 50 nm thick spin-coated at 2000 rpm for 50 s and baked at 120 °C for 30 min to dry. Methanofullerenes and P3HT in the equal weight ratio were mixed and dissolved in *o*-DCB solution at the concentration of 17 mg·mL^{-1}. The solution was then spin-coated onto the top of PEDOT:PSS at 900, 1000, and 1100 rpm for 60 s, respectively. For all devices, the active layer has a thickness of around 100 nm. Time for solvent annealing (SA) was at least 60 min. Al was then deposited on the active layer. The deposition rates were usually 0.05−0.10 nm·s^{-1}, and the thickness of the evaporation layers were monitored by a thickness/rate meter (MBraun). After cathode was deposited, the devices were post-thermally annealed (PTA) at 110 °C for 10 min before cooling down to room temperature under nitrogen in glovebox. The crossing area of 0.18 cm^2 between the cathode and the anode was defined as active device area. All fabrication steps after the deposition of PEDOT:PSS layer were carried out in a nitrogen glovebox with H_2O < 0.1 ppm and O_2 <0.1 ppm. The I−V characteristics in the dark and under illumination were measured. Photocurrent was measured under a solar simulator with AM 1.5G illumination (100 mW·cm^{-2}) in glovebox.

RESULTS AND DISCUSSION

UV−Vis Solution Absorption. The UV−vis spectra of the fullerene derivatives in 10^{-5} M toluene solution were shown in Figure 3 and Table 1 in calibration to concentration. The spectra showed that the absorption of C_{70} compounds were stronger than its C_{60} homologues, and bisadducts were stronger than its monoadduct homologues in 400−800 nm, which is consistent with the literature.[17,24] The absorption of **A1** was almost the same as that of $PC_{61}BM$, especially the featured peaks at 434 and 696 nm. The same absorption characteristics of A1 and $PC_{61}BM$ indicated that the structure changing from methyl ester to *n*-dibutylamide had little effect on the electronic properties of the whole molecule, which was consistent with its E_{red}^{1onest} tested by cyclic voltammetry and our previous work.[15] **A2**, **B1**, and **B2** have no distinct and sharp absorption band, but with broad band instead, there were several isomers in the three fullerene derivatives convinced by ^{1}H NMR, ^{13}C NMR, and HPLC.

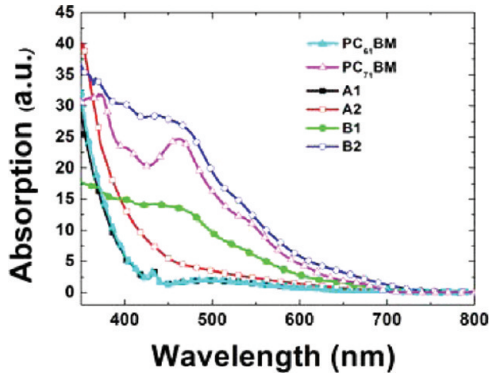

Figure 3. UV−vis absorption spectra of fullerene solution in toluene at 10^{-5} M, calibrated by concentration. Solid symbols stand for monoadduct derivatives, and hollow symbols stand for bisadduct derivatives.

Table 1. UV-Vis Absorbance Peak or Broad Band Data[a]

fullerene	400−450 (nm)	450−600 (nm)	>500 (nm)
$PC_{61}BM$	434		698
A1	434		699
A2	433	497	698
$PC_{71}BM$	463	462, 540	673
B1		486	
B2		497	699

[a]UV-vis absorption was tested in toluene solution at RT.

Electrochemistry Properties. The electrochemical property is one of the most important properties of fullerenes. The gap between the LUMO level of the donor and acceptor provides the driving force for the charge dissociation of the excitons in the polymer donor to overcome the binding energy of the excitons. The value of the difference between the LUMO level of the acceptor and the HOMO level of the donor determines V_{oc}.[10,33] The value of the difference between the HOMO levels of the donor and acceptor provides the driving force for the dissociation of the excitons in the acceptor. The energy level alignment between four fullerene derivatives and regioregular P3HT assures that there are good charge-transfer

dx.doi.org/10.1021/am2016975 | ACS Appl. Mater. Interfaces 2012, 4, 1065−1071

and charge-separate states in the donor/acceptor blends (Figure S3, Supporting Information).[34,35] The LUMO level of all the fullerene derivatives was measured by cyclic voltammetry (as shown in Table 2 and Figure 4) and estimated from their onset value of the first reduction (E_{red}^{1onest}) by eq 1.

Table 2. Electrochemistry Properties of Fullerene Derivatives[a]

fullerene	E_{red}^{1onest} (V)	LUMO (eV)	Δ (eV)
$PC_{61}BM$	−1.09	−3.71	0.00
$PC_{71}BM$	−1.10	−3.70	0.01
A1	−1.11	−3.69	0.02
A2	−1.14	−3.66	0.05
B1	−1.11	−3.69	0.02
B2	−1.20	−3.61	0.10

[a]Measurement parameters: E_{red}^{1onest} was in V vs Fc/Fc^+; 10^{-4} to 10^{-3} M in *o*-DCB solution; supporting electrolyte, tetrabutyl ammonium hexafluorophosphate ($TBAPF_6$, 0.1 M); working electrode, glassy carbon; counter electrode, Pt wire; reference electrode, Ag wire; internal reference, 0.3 mg c.a. A.R. ferrocene by Soxhlet extracted; scan rate, 50 $mV{\cdot}s^{-1}$; temperature, room temperature 25 °C c.a.; Δ was compared to $PC_{61}BM$'s LUMO level.

$$\text{LUMO} = -\,e(E_{red}^{1onest} + 4.80)(\text{V vs Fc/Fc}^+) \quad (1)$$

A1, with *n*-dibutyl amide group instead of methyl ester of PCBM, has almost the same E_{red}^{1onest} as $PC_{61}BM$; *n*-dibutyl amide group has little effect on the electrochemistry properties of fullerene, in line with UV comparison of **A1** and $PC_{61}BM$, which is in agreement with our previous report.[15] Differential pulse voltammetry (DPV) is a sensitive and semiquantitative electrochemistry method to determine the electrochemical properties. Symmetrical peaks of E_{pa} and E_{pc}, equal i_{pa} and i_{pc}, and three sharp and equal intensity peaks of DPV showed that **A1** was a typical reversible fullerene derivative. The equal E_{red}^{1onest} of **A1** and **B1** as $PC_{61}BM$ and $PC_{71}BM$ was attributed to the relief of strain and pyracylene-type electronic of [70] fullerene derivatives.[36] The E_{red}^{1} of **A2**, **B1**, and **B2** were quasi-reversible while the E_{red}^{2} and E_{red}^{3} of them were obviously semireversible as indicated by the asymmetric peaks of E_{pa} and E_{pc} and unequal value of i_{pa} and i_{pc}. which also can be demonstrated by the existence of double or multipeaks from DPV curves. These results further confirmed the existence of isomers in these derivatives.[23]

Photovoltaic Properties. The PCE of the monoadduct fullerene based OPVs performed better than the bisadduct ones, i.e., **A1** > **A2** and **B1** > **B2**. We had expected that **A2** and **B2** would have more excellent performance than their monoadducts, as both **A2** and **B2** with LUMO level 0.02 and 0.10 eV higher than that of PCBM (Figure 5 and 6, Table S6, Supporting Information). Unfortunately, whether SA and PTA were used or not, the PCE of **A2** and **B2** based OPVs were very low. The V_{oc} of the devices based on **A2** was slightly lower than that of **A1** while **B2**'s V_{oc} drops dramatically compared with that based on **B1**. Notably, the J_{sc} of the **B1** and **B2** based device were very low, which were similar to that of the $TriPC_{61}BM$ as reported.[26]

The number of isomers of **A2** and **B2** indicated by HPLC were 5 and 5, respectively, at least, because there were too broad peaks in HPLC figures to recognize how many there were (Figure 2). The more addition, the smaller mobility of multiaddcut had.[26] A possible explanation for this decrease was

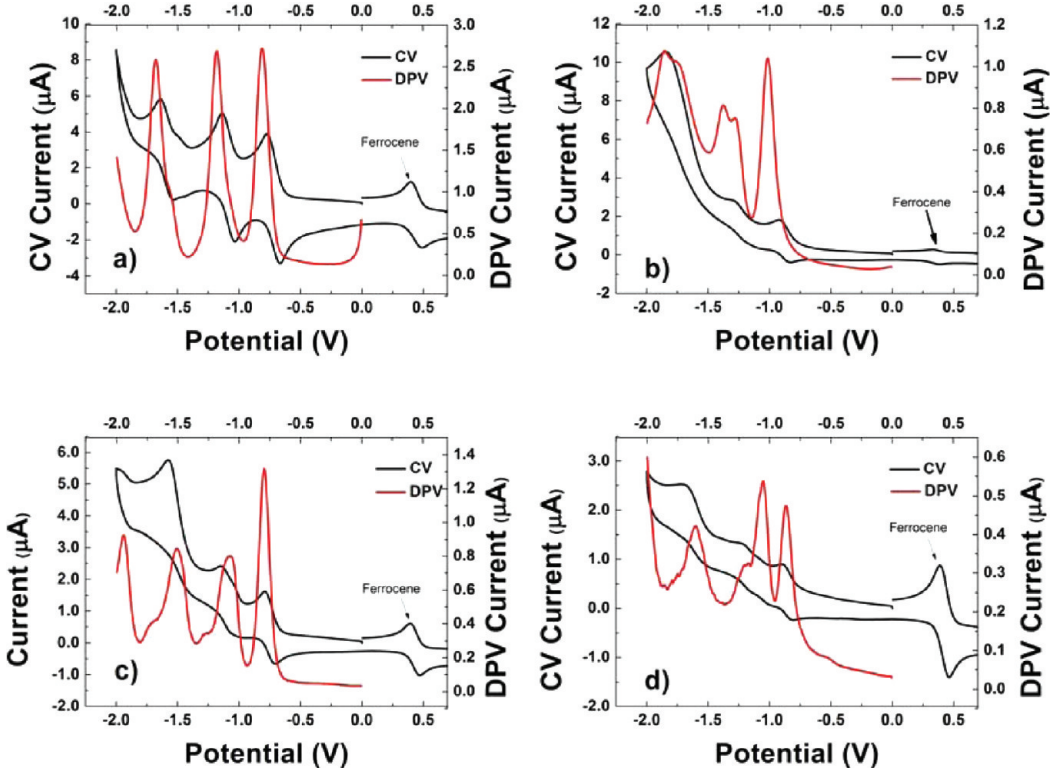

Figure 4. CV and DPV figures of four fullerene derivatives. The parameters of CV were listed in the caption of Table 2. DPV were tested in the same cell as CV did. The parameters of DPV: amplitude, 0.05 V; pulse width, 0.2 s; sample width, 0.0167 s; pulse period, 0.5 s. (a) **A1**; (b) **A2**; (c) **B1**; (d) **B2**.

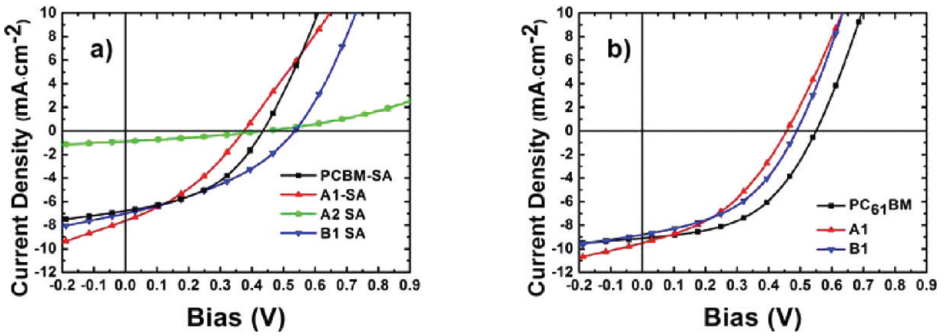

Figure 5. $J-V$ curves of P3HT/fullerene devices under AM 1.5G illumination at 100 mW·cm^{-2}.(a) SA treatment; (b) SA and PTA treatment. The $J-V$ curves of **B2** with SA treatment; **A2** and **B2** with SA and PTA treatment were not shown because they were almost lying on the X axis.

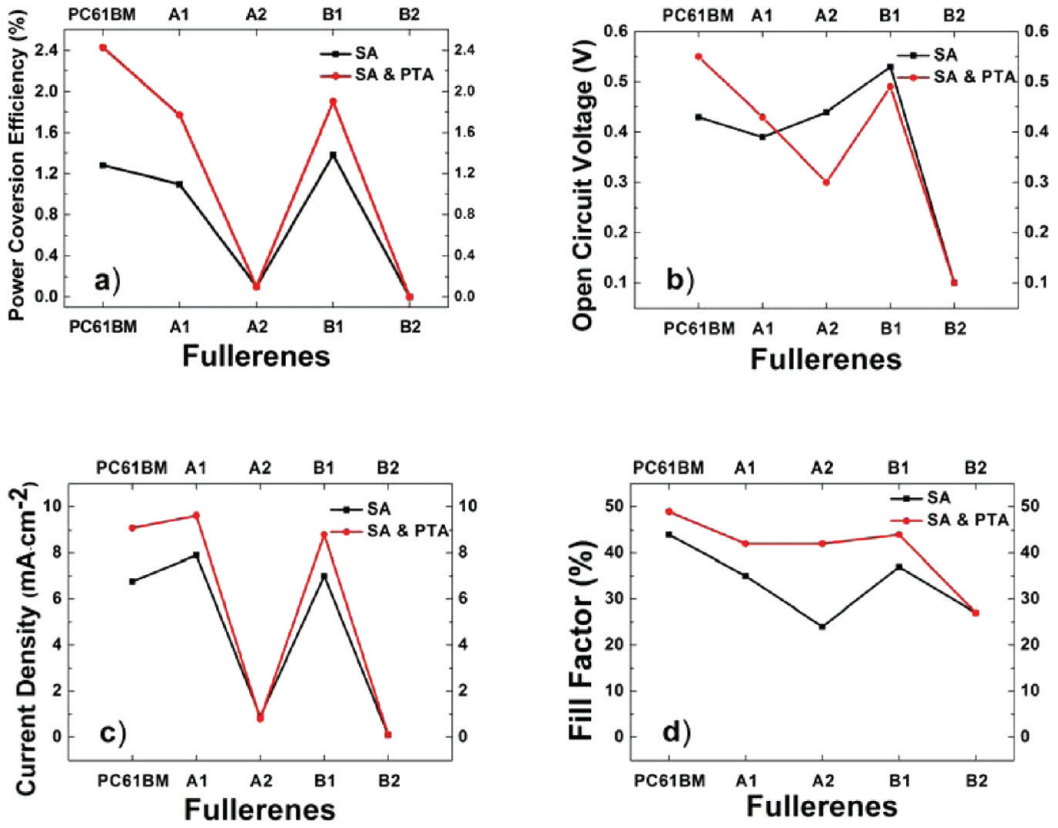

Figure 6. Device indices of each fullerene based OPVs in the condition of SA and SA and PTA. (a) power conversion efficiency(PCE); (b) open circuit voltage (V_{oc}); (c) current density (J_{sc}); (d) fill factor (FF).

that macroscopic mobility was the average of all orientation, and isomers increased the disorder strongly; thus, **A2** and **B2** of at least 5 isomers, respectively, may have very low mobility leading to very low J_{sc}.

Surface morphology study by AFM technology was not consistent with the whole phase situation in 3D structure, because the polymer/fullerene film was not homogeneous vertically supported by neutron scattering,[37] while it is a good and readily available method to reveal the phase separation to some content. Phase images showed the scale of phase separation; it is believed that the scale surrounding 10 nm had the maximum effect on exciton diffusion and dissociation.[38] Moreover, the film roughness indicated by height images reveals the quality of film with the index of root-mean-square roughness (rms). The phase images with SA treatment and SA and PTA treatment were shown in Figures 7 and 8, and rms was listed in Figure 9.

Although none of the scale of phase separation was smaller than 10 nm, usually bigger than 50 nm, the phase images were almost consistent with the device performance. **A2** and **B2** based devices had a phase separation scale of 80 to 200 nm; the phase was very nonuniform. On the other hand, **A1** and **B1** based devices had a phase separation scale of 50 to 70 nm, and **B1**'s was much more ordered than **A1**'s with small continuous blocks. After PTA treatment, **A1** and **B1**'s phase separation was decreased about 10 nm, and **B1** formed a nanoisland at about 40 to 60 nm. **A2**'s phase separation was more unordered and at large scale. Surprisingly, **B2** based film showed ordered and small scale phase separation but low device performance, which was an analogue with early multiadduct fullerene literature.[39] rms showed a similar trend. PTA treatment decreased the film

dx.doi.org/10.1021/am2016975 | ACS Appl. Mater. Interfaces 2012, 4, 1065−1071

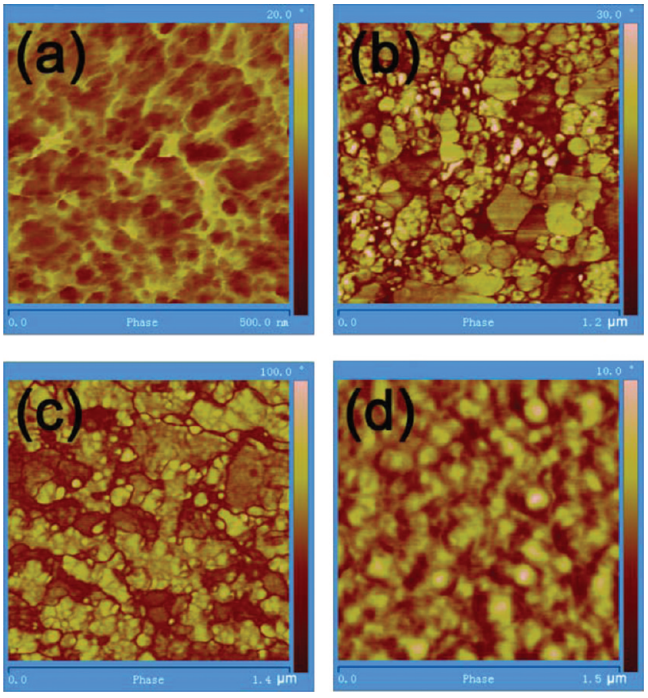

Figure 7. AFM phase images of four fullerene based OPVs with SA treatment in tapping mode. (a) **A1**; (b) **A2**; (c) **B1**; (d) **B2**.

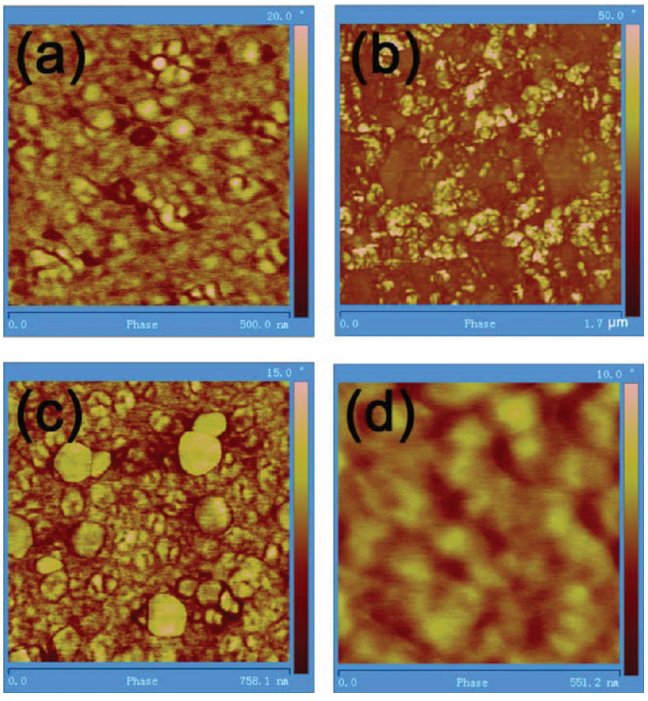

Figure 8. AFM phase images of four fullerene based OPVs with SA and PTA treatment in tapping mode. (a) **A1**; (b) **A2**; (c) **B1**; (d) **B2**.

roughness of **A1** and **B1** based devices notably, but **A2** and **B2** have no similar trend; even **A2**'s rms increased, suggesting that PTA treatment can improve film quality.

CONCLUSION

We synthesized four [6,6]-phenyl-C_{61} and C_{71} butylsaure *n*-dibutyl amide (PCBDBA) fullerene derivatives, and the photovoltaic cells were fabricated with P3HT. The hetero-junction organic photovoltaics showed device performance for two monoadducts **A1** and **B1**, which have PCE of 1.77% and 1.90%, respectively, near PCBM's 2.43%. Our results also indicate that more adducts of fullerenes afford lower efficiency, even resulting in broken circuit. This is due to the fact that multiadduct has lower mobility, larger scale of phase separation, and higher rms than monoadducts. It is demonstrated that the products were good models to study the structure performance of the monoadduct and bisadduct fullerene materials for revealing the relationship between C_{60} and C_{70} monoadduct and bisadduct derivatives and providing the logos on how to design fullerene materials for this purpose. It may have great potential for further applications on optoelectronic devices based on π-conjugated conducting polymers in various fields.

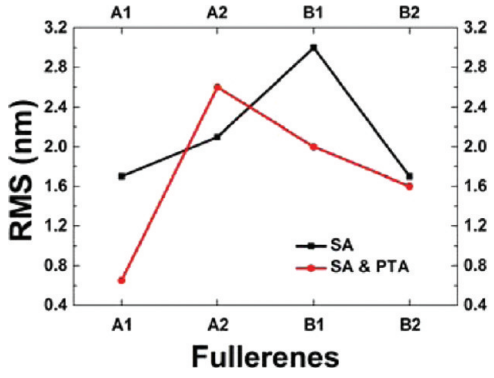

Figure 9. rms of four fullerene based OPVs with SA and PTA treatment in tapping mode calculated by AFM height images in 1.5 μm c.a. area.

ASSOCIATED CONTENT

Supporting Information

Details of synthesis, NMR, IR, MS, HPLC, TG/DTA, equipment, and reagents. This material is available free of charge via the Internet at http://pubs.acs.org.

AUTHOR INFORMATION

Corresponding Author

*Yuliang Li: fax, 86-10-82616576; tel, 86-10-62588934; e-mail, ylli@iccas.ac.cn. Shengqiang Xiao: fax, 86-27-87879468; tel, 86-27-87870537; e-mail, shengqiang@whut.edu.cn.

ACKNOWLEDGMENTS

This work was supported by the National Nature Science Foundation of China (21031006, 10874187, 20831160507), the NSFC-DFG joint fund (TRR61), and the National Basic Research 973 Program of China. The solar cell fabrication and test were financially supported by self-determined and innovative research funds of WUT (2011-II-009). Prof. S.X. is also thankful for the financial support from the State Key Lab of Advanced Technology for Materials Synthesis and Processing (2009-PY-1).

REFERENCES

(1) Wong, W. Y.; Wang, X. Z.; He, Z.; Djurisic, A. B.; Yip, C. T.; Cheung, K. Y.; Wang, H.; Mak, C. S. K.; Chan, W. K. *Nat. Mater.* **2007**, *6*, 521−527.

(2) Zhan, X. W.; Tan, Z. A.; Domercq, B.; An, Z. S.; Zhang, X.; Barlow, S.; Li, Y. F.; Zhu, D. B.; Kippelen, B.; Marder, S. R. *J. Am. Chem. Soc.* **2007**, *129*, 7246−7247.

(3) Hou, J.; Chen, H.-Y.; Zhang, S.; Li, G.; Yang, Y. *J. Am. Chem. Soc.* **2008**, *130*, 16144−16145.
(4) Qin, R.; Li, W.; Li, C.; Du, C.; Veit, C.; Schleiermacher, H.-F.; Andersson, M.; Bo, Z.; Liu, Z.; Inganäs, O.; Wuerfel, U.; Zhang, F. *J. Am. Chem. Soc.* **2009**, *131*, 14612−14613.
(5) Son, H. J.; Wang, W.; Xu, T.; Liang, Y.; Wu, Y.; Li, G.; Yu, L. *J. Am. Chem. Soc.* **2011**, *133*, 1885−1894.
(6) Park, S. H.; Roy, A.; Beaupre, S.; Cho, S.; Coates, N.; Moon, J. S.; Moses, D.; Leclerc, M.; Lee, K.; Heeger, A. J. *Nat. Photonics* **2009**, *3*, 297−303.
(7) Fan, H.; Zhang, M.; Guo, X.; Li, Y.; Zhan, X. *ACS Appl. Mater. Interfaces* **2011**, *3*, 3646−3653.
(8) Service, R. F. *Science* **2011**, *332*, 293.
(9) Shin, W. S.; Lee, J. C.; Kim, J. R.; Lee, H. Y.; Lee, S. K.; Yoon, S. C.; Moon, S. J. *J. Mater. Chem.* **2011**, *21*, 960−967.
(10) Brabec, C. J.; Cravino, A.; Meissner, D.; Sariciftci, N. S.; Fromherz, T.; Rispens, M. T.; Sanchez, L.; Hummelen, J. C. *Adv. Funct. Mater.* **2001**, *11*, 374−380.
(11) Kennedy, R. D.; Ayzner, A. L.; Wanger, D. D.; Day, C. T.; Halim, M.; Khan, S. I.; Tolbert, S. H.; Schwartz, B. J.; Rubin, Y. *J. Am. Chem. Soc.* **2008**, *130*, 17290−17292.
(12) Popescu, L. M.; van't Hof, P.; Sieval, A. B.; Jonkman, H. T.; Hummelen, J. C. *Appl. Phys. Lett.* **2006**, *89*, 213507.
(13) Kooistra, F. B.; Knol, J.; Kastenberg, F.; Popescu, L. M.; Verhees, W. J. H.; Kroon, J. M.; Hummelen, J. C. *Org. Lett.* **2007**, *9*, 551−554.
(14) Zheng, L. P.; Zhou, Q. M.; Deng, X. Y.; Yuan, M.; Yu, G.; Cao, Y. *J. Phys. Chem. B* **2004**, *108*, 11921−11926.
(15) Liu, C.; Li, Y.; Li, C.; Li, W.; Zhou, C.; Liu, H.; Bo, Z.; Li, Y. *J. Phys. Chem. C* **2009**, *113*, 21970−21975.
(16) Sukeguchi, D.; Singh, S. P.; Reddy, M. R.; Yoshiyama, H.; Afre, R. A.; Hayashi, Y.; Inukai, H.; Soga, T.; Nakamura, S.; Shibata, N.; Toru, T. *Beilstein J. Org. Chem.* **2009**, *5*, 10.
(17) Mikroyannidis, J. A.; Kabanakis, A. N.; Sharma, S. S.; Sharma, G. D. *Adv. Funct. Mater.* **2011**, *21*, 746−755.
(18) Matsuo, Y.; Sato, Y.; Niinomi, T.; Soga, I.; Tanaka, H.; Nakamura, E. *J. Am. Chem. Soc.* **2009**, *131*, 16048−16050.
(19) Hsieh, C. H.; Cheng, Y. J.; Li, P. J.; Chen, C. H.; Dubosc, M.; Liang, R. M.; Hsu, C. S. *J. Am. Chem. Soc.* **2010**, *132*, 4887−4893.
(20) Meng, X.; Zhang, W.; Tan, Z. A.; Du, C.; Li, C.; Bo, Z.; Li, Y.; Yang, X.; Zhen, M.; Jiang, F.; Zheng, J.; Wang, T.; Jiang, L.; Shu, C.; Wang, C. *Chem. Commun.* **2012**, *48*, 425−427.
(21) Susarova, D. K.; Khakina, E. A.; Troshin, P. A.; Goryachev, A. E.; Sariciftci, N. S.; Razumov, V. F.; Egbe, D. A. M. *J. Mater. Chem.* **2011**, *21*, 2356−2361.
(22) Mikroyannidis, J. A.; Tsagkournos, D. V.; Sharma, S. S.; Sharma, G. D. *J. Phys. Chem. C* **2011**, *115*, 7806−7816.
(23) Echegoyen, L.; Echegoyen, L. E. *Acc. Chem. Res.* **1998**, *31*, 593−601.
(24) Choi, J. H.; Son, K.-I.; Kim, T.; Kim, K.; Ohkubo, K.; Fukuzumi, S. *J. Mater. Chem.* **2010**, *20*, 475−482.
(25) Padinger, F.; Brabec, C. J.; Fromherz, T.; Hummelen, J. C.; Sariciftci, N. S. *Opto-Electron. Rev.* **2000**, *8*, 280−283.
(26) Lenes, M.; Shelton, S. W.; Sieval, A. B.; Kronholm, D. F.; Hummelen, J. C.; Blom, P. W. M. *Adv. Funct. Mater.* **2009**, *19*, 3002−3007.
(27) Lenes, M.; Wetzelaer, G. J. A. H.; Kooistra, F. B.; Veenstra, S. C.; Hummelen, J. C.; Blom, P. W. M. *Adv. Mater.* **2008**, *20*, 2116−2119.
(28) Liu, Y.; Xiao, S.; Li, H.; Li, Y.; Liu, H.; Lu, F.; Zhuang, J.; Zhu, D. *J. Phys. Chem. B* **2004**, *108*, 6256−6260.
(29) Li, Y.; Liu, Y.; Wang, N.; Li, Y.; Liu, H.; Lu, F.; Zhuang, J.; Zhu, D. *Carbon* **2005**, *43*, 1968−1975.
(30) Liu, Y.; Yang, C. H.; Li, Y. J.; Li, Y. L.; Wang, S.; Zhuang, J. P.; Liu, H. B.; Wang, N.; He, X. R.; Li, Y. F.; Zhu, D. B. *Macromolecules* **2005**, *38*, 716−721.
(31) Hummelen, J. C.; Knight, B. W.; LePeq, F.; Wudl, F.; Yao, J.; Wilkins, C. L. *J. Org. Chem.* **1995**, *60*, 532−538.
(32) Wang, J.-L.; Duan, X.-F.; Jiang, B.; Gan, L.-B.; Pei, J.; He, C.; Li, Y.-F. *J. Org. Chem.* **2006**, *71*, 4400−4410.
(33) Scharber, M. C.; Wuhlbacher, D.; Koppe, M.; Denk, P.; Waldauf, C.; Heeger, A. J.; Brabec, C. L. *Adv. Mater.* **2006**, *18*, 789−794.
(34) Maurano, A.; Hamilton, R.; Shuttle, C. G.; Ballantyne, A. M.; Nelson, J.; O'Regan, B.; Zhang, W.; McCulloch, I.; Azimi, H.; Morana, M.; Brabec, C. J.; Durrant, J. R. *Adv. Mater.* **2010**, *22*, 4987−4992.
(35) Clarke, T. M.; Durrant, J. R. *Chem. Rev.* **2010**, *110*, 6736−6767.
(36) Allemand, P. M.; Koch, A.; Wudl, F.; Rubin, Y.; Diederich, F.; Alvarez, M. M.; Anz, S. J.; Whetten, R. L. *J. Am. Chem. Soc.* **1991**, *113*, 1050−1051.
(37) Kiel, J. W.; Kirby, B. J.; Majkrzak, C. F.; Maranville, B. B.; Mackay, M. E. *Soft Matter* **2010**, *6*, 641−646.
(38) Thompson, B. C.; Frechet, J. M. J. *Angew. Chem., Int. Ed.* **2008**, *47*, 58−77.
(39) Gebeyehu, D.; Brabec, C. J.; Padinger, F.; Fromherz, T.; Hummelen, J. C.; Badt, D.; Schindler, H.; Sariciftci, N. S. *Synth. Met.* **2001**, *118*, 1−9.